Coulomb interactions and effective quantum inertia of charge carriers in a macroscopic conductor

Adrien Delgard, Boris Chenaud, Ulf Gennser, Antonella Cavanna, D. Mailly, P. Degiovanni, Christophe Chaubet

Coulomb interactions and effective quantum inertia of charge carriers in a macroscopic conductor

A. Delgard[1], B. Chenaud[1], U. Gennser[2], A. Cavanna[2], D. Mailly[2], P. Degiovanni[3] and C. Chaubet[1]
[1] *Université Montpellier 2, CNRS, Laboratoire Charles Coulomb UMR5221, F-34095, Montpellier, France*
[2] *Centre de Nanosciences et de Nanotechnologies (C2N), CNRS, Université Paris-Sud, Université Paris-Saclay, 91120 Palaiseau, France and*
[3] *Univ Lyon, Ens de Lyon, Université Claude Bernard Lyon 1, CNRS, Laboratoire de Physique, F-69342 Lyon, France.**

We study the low frequency admittance of a quantum Hall bar of size much larger than the electronic coherence length. We find that this macroscopic conductor behaves as an ideal quantum conductor with vanishing longitudinal resistance and purely inductive behavior up to $f \lesssim 1\,\mathrm{MHz}$. Using several measurement configurations, we study the dependence of this inductance on the length of the edge channel and on the integer quantum Hall filling factor. The experimental data are well described by a scattering model for edge magnetoplasmons taking into account effective long range Coulomb interactions within the sample. We find that the inductance's dependence on the filling factor arises predominantly from the effective quantum inertia of charge carriers induced by Coulomb interactions.

PACS numbers: 72.10.-d, 73.23.-b,73.43.-f, 73.43.Fj

By demonstrating that macroscopic conductors could exhibit robust d.c. transport properties of quantum origin, the integer quantum Hall effect (IQHE) [1**?** –4] has been a major surprise. The importance of this breakthrough for metrology was acknowledged immediately [1] and has lead to the redefinition of the Ohm [5**?**]. The finite frequency response of quantum Hall conductors has been intensively studied by metrologists: the use of an a.c. bridge at finite frequency f revealed departure of the Hall resistance $R_H(f)$ at $\nu = 2$ from the expected value $R_K/2 = h/2e^2$ [6–10]. It was then attributed to "intrinsic inductances and capacitances" [11, 12]. Later, Schurr *et al* proposed a double shielded sample allowing for a frequency-independent resistance standard [13], but these works left open the question of the origin of these capacitances and inductances.

On the other hand, the finite frequency transport properties of quantum coherent conductors, of size smaller than the electron coherence length, are expected to be dominated by quantum effects. For low-dimensional conductors such as carbon nanotubes [14], or graphene [15], the inductance is of purely kinetic origin. Small superconducting inductors [16, 17] now used in space industry [18] are based on the inertia of Cooper pairs. For a quantum coherent conductor, the theory developed by Bűttiker and his collaborators [19–21] relates the associated L/R or RC times to the Wigner-Smith time delay for charge carriers scattering across the conductor. These remarkable predictions have been confirmed by the measurement of the finite frequency admittance of quantum Hall R-C [22] and R-L [23, 24] circuits of µm-size in the GHz range at cryogenic temperatures.

In this Letter, we demonstrate that, in the a.c. regime, a mm long ungated macroscopic quantum Hall bar, of size much larger than the electronic coherence length, exhibits a finite inductance as well as a vanishing longitudinal resistance. Such a purely inductive longitudinal response is expected for quantum conductors with zero backscattering: a kinetic energy cost proportional to the square of the current arises from both the Pauli principle and the linear dispersion relation for electrons close to the Fermi level (see Sec. I of Suppplemental Material at [**?**]). This effective inertia of carriers causes the current response to lag the applied electric field. Here, we identify an inductance of the order of tens of $\mu\mathrm{H\,mm^{-1}}$ and connect it to an effective velocity v_{eff} along the quantum Hall bar's edges. Contrary to gated samples, in which v_{eff} is almost independent of the filling factor ν [23], we show that, because of Coulomb interactions between opposite edges of the sample, v_{eff} depends on ν in our samples. Using the edge-magnetoplasmon scattering approach combined with a discrete element approach *à la* Bűttiker, we show that:

$$\frac{v_{\mathrm{eff}}(\nu)}{v_{\mathrm{d}}(\nu)} = 1 + \frac{\nu\alpha_{\mathrm{eff}}(\nu)}{\pi}\ln\left[\frac{W/\xi_H(\nu)}{\nu}\right] \qquad (1)$$

for a sample of width W. Here, $v_{\mathrm{d}}(\nu)$ represents the charge density wave velocity along the system of ν-copropagating chiral edge channels, neglecting Coulomb interactions with the other (counter-propagating) edge channels. In a Büttiker view of the edge channels [25] as well as in models assuming that no compressible stripes are present at the edge [**?** **?**], $v_{\mathrm{d}}(\nu)$ is the drift velocity of non-interacting electrons at the edge in an effective confining potential U_ν and, therefore, it plays the role of an effective Fermi velocity in the 1D linear dispersion relation along the edge [26]. In the presence of compressible stripes, which appear for a sufficiently smooth confining potential [27], it corresponds to the effective velocity of the charge density mode in the system of ν copropagating edge channels [28], taking into account the presence

* Corresponding Author : christophe.chaubet@umontpellier.fr

of the incompressible part of the edge channel [29]. Nevertheless, we denote it by $v_{\rm d}(\nu)$ because, in a model of an edge channel without compressible parts, it really would be an electronic drift velocity. Importantly, this velocity deviates from from the classical $1/B$ behavior of the electronic drift velocity because of screening effects, which change the electrostatic potential at the edge as ν varies.

Here, $\alpha_{\rm eff}(\nu)$ denotes the effective fine structure constant ($\alpha_{\rm qed}$ in the vacuum) at filling factor ν: $\alpha_{\rm eff}(\nu) = (\alpha_{\rm qed}/\varepsilon_r) \times (c/v_{\rm d}(\nu))$. The length $\xi_H(\nu)$, which also depends on ν, is an effective renormalized width of a single edge channel of the order of the width of incompressible edge channels $\lambda_H(\nu)$ [27] (see Sec. IV of the Suppplemental Material at [**?**]).

Our work demonstrates that the purely inductive response of the macroscopic ungated quantum Hall bar reflects the effective quantum inertia of charge carriers renormalized by Coulomb interactions within the sample. Therefore, although electron transport across such a conductor is not coherent, its d.c. and a.c. transport properties are of quantum origin, a fact that ultimately relies on the coherence of edge-magnetoplasmon (EMP) modes propagating along chiral edge channels. EMP coherence has enabled the demonstration of single and double EMP Fabry-Pérot interferometers [30] as well as of a Mach-Zehnder plasmonic interferometer [31].

Using shallow etching, our samples are processed on an AlGaAs/GaAs heterojunction with the two dimensional electron gas (2DEG) located at the heterointerface (105 nm beneath the surface) with carrier density $n_s = 5.1 \times 10^{11}\,{\rm cm}^{-2}$ and mobility $\mu = 30\,{\rm m}^2/{\rm Vs}$. We have processed a $2 \times 0.4{\rm mm}^2$ ungated Hall bar which exhibits a sufficiently large kinetic inductance. The sample has no back gate and is glued on a ceramic sample holder to avoid parasitic capacitances. It is placed at the center of a high magnetic field at 1.5 K.

In the measurement setup depicted on Fig. 1-a., the current is injected using $H_{\rm cur}$ (5 mV bias), and measured using $L_{\rm cur}$. The potential of $H_{\rm pot}$ is measured while $V = 0$ and $I = 0$ are imposed at $L_{\rm pot}$. The current intensity ($\lesssim 0.5\,\mu$A at $\nu = 2$) remains below the breakdown current and currents used in metrology [6**?**]. For each values of B, the resistance and the reactance have been measured for 300 values of the frequency f in the range 40 Hz-100 kHz.

Due to chirality of the quantum Hall transport, an ohmic contact wire-bonded to the sample holder and so to a coaxial cable, generates a leakage current through the cable capacitance if the potential does not vanish [34, 35]. This results in a faulty measurement [36, 37]. For this reason, all results presented here have been carried out at integer filling factors, where the longitudinal resistance $R_{xx}(\omega)$ vanishes[38]. Furthermore, only 3 of the ohmic contacts processed on the sample were wire-bonded onto the sample holder as shown on Fig. 1.b. To measure a zero resistance state, the third contact is inserted along the edge connected to the reference potential. In d.c., one would measure a potential $V_{\rm H_{pot}} = 0$. In a.c.,

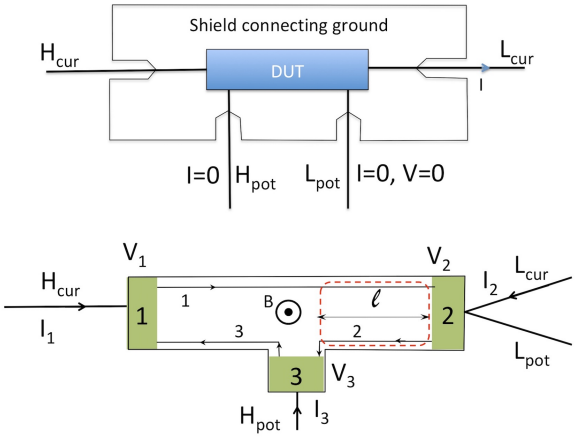

FIG. 1. a) The Device Under Test (DUT) is measured using four coaxial cables and the impedance-meter Agilent HP4294A, which measures the current I at $L_{\rm cur}$, the potential V at $H_{\rm pot}$, and gives $G = I/V$, for details see Ref. [32, 33]. Note that the potentials of $H_{\rm pot}$, $L_{\rm pot}$, $H_{\rm cur}$ and $L_{\rm cur}$ are the potentials of the four connectors of the impedance-meter. b) Scheme of the multi-terminal Hall bar with only three ohmic contacts wire-bonded onto the sample holder. In this geometry, the impedance is $Z_{23}^{(\rm expt)}(\omega) = -(\partial V_3/\partial I_2)(\omega)$ for $V_2 = 0$.

$V_{\rm H_{pot}} \neq 0$ and we measure the frequency dependent impedance $Z_{23}^{(\rm expt)}(\omega) = -\,\partial V_3/\partial I_2|_{V_2=0}\,(\omega)$. Different configurations and edge channel lengths can be obtained by recabling the contacts and changing the sample side (in this case, the magnetic field orientation must be reversed). We have also wire-bonded a fourth ohmic contact on the same side of the sample to connect $L_{\rm pot}$ to access another edge channel length.

Figure 2 presents unfiltered and non-averaged raw data for the reactance $X(f) = {\rm Im}(Z_{23}^{(\rm expt)}(2\pi f))$ in a given sample configuration for $\nu = 2$, 4, 6 and 8. The positive linear dependence of $X(f)$ is the signature of an inductive behavior. The corresponding inductance decreases with ν. These data are completely reproducible in the regions of magnetic fields where $R_{xx} = 0$. This is a key point of our work: for integer filling factors, the real part $R(f) = {\rm Re}(Z_{23}^{(\rm expt)}(2\pi f))$ of the measured impedance is close to zero with values between $\pm 0.5\,\Omega$ at low frequency as shown in the inset of Fig. 2. These results extend the work of Gabelli *et al* [23] in which the sample resistance was $R_H = R_K/\nu$, to the case of a zero resistance macroscopic device. At higher frequencies, a small real part of the measured response function $R(f)$ appears. This effect is discussed in Sec. II of Suppplemental Material at [**?**] and is related to the deviation of the reactance $X(f)$ from linearity seen on Fig. 2.

Since the ac transport properties of a quantum Hall conductor is directly related to the scattering of edge-magnetoplasmons [39–42], already used to study EMP propagation [43, 44], charge fractionalization [45–48], and electronic relaxation and decoherence [49–51], we have developed an analytical model (see Sec. III in Suppple-

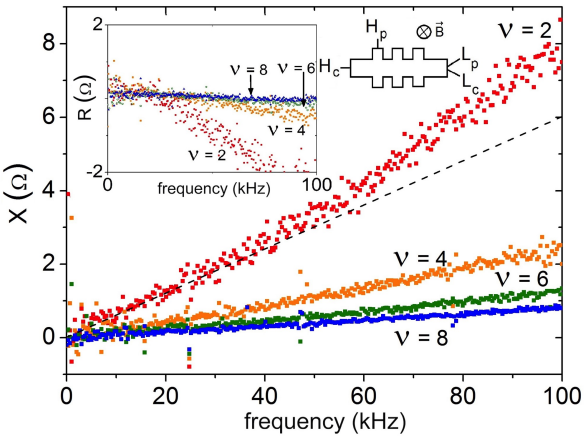

FIG. 2. The reactance X as a function of the frequency f for different ν and $B_{<0}$, in the measurement configuration shown here. Inset: the longitudinal resistance $R(f)$ vanishes quadratically for integer filling factors at low frequency.

mental Material at [**?**]) in the spirit of Ref. [30] for scattering of EMP modes in a quantum Hall bar taking into account long range inter-channel Coulomb interactions. It assumes that, in our ungated quantum Hall bars, all edge channels of same chirality have the same velocity $v_{\rm d}(\nu)$ and are so strongly coupled that they see the same time dependent potential as in Ref. [24]. Since edge states are distant from more than 1.5 cm from shield of coaxial cables located beneath the sample holder, estimated parasitic capacitance to shield for edge states is below 1 fF while the inter-edge capacitance c_H is of the order of 0.1 pF. Therefore, Coulomb interactions effects are dominated by the inter-edge capacitance C_H. Finally, dissipation of EMP modes have been neglected, an hypothesis a posteriori satisfied in our samples.

In the geometry depicted on Fig. 1, the low frequency expansion of the measured reactance is of the form:

$$\mathrm{Im}\left(Z_{23}^{(\rm expt)}(\omega)\right) = \mathrm{i}L\omega + \mathcal{O}(\omega^2) \tag{2}$$

where L denotes the total inductance for the quantum Hall bar delimited by a dashed red box on Fig. 1-b. Because here, the magnetic inductance is much smaller than the kinetic inductance (see Suppplemental Material at [**?**], Sec. I), L can be obtained from the edge magnetoplasmon scattering model as

$$L = (R_K/\nu) \times (l/2\, v_{\rm eff}(\nu)) \tag{3a}$$

$$v_{\rm eff}(\nu) = v_{\rm d}(\nu) \times \left(1 + \frac{C_q(\nu)}{2C_H(\nu)}\right). \tag{3b}$$

where l is the length of the Hall bar (see Fig. 1-b), $C_q(\nu) = \nu e^2 l/h v_{\rm d}(\nu)$ is the quantum capacitance of ν edge channels recently measured in Corbino geometries [52], and the geometric capacitance $C_H(\nu)$ describes the effect of Coulomb interactions between counter-propagating edge channels. This is different from the quantum RL-circuit where, because of the gating, the capacitance C_H has to be replaced by the capacitance C_g with the nearby gates leading to a renormalization of $v_{\rm d}$ by $1 + C_q/C_g$ for right and left moving charge density waves [23]. Here, the renormalization factor involves a C_H capacitance with the series addition $C_q/2$ of the quantum capacitances of counter-propagating edges. As a consequence, Eq. (3) still relates $L = R_H^2 C_\mu$ to the Hall resistance and to the electrochemical capacitance [53] C_μ defined as the series addition of C_H to $C_q/2$. Eq. (3) suggests that the inductance can be interpreted as a kinetic inductance associated with an effective time of flight $l/v_{\rm eff}(\nu)$. But, as discussed in Suppplemental Material at [**?**] (Sec. III), $v_{\rm eff}(\nu)$ is neither the drift velocity for non-interacting electrons nor even a renormalized electron's velocity within chiral edge channels, but an effective velocity arising from the combination of their kinetic quantum inertia and Coulomb interactions within the quantum Hall bar. This effective inertia is of quantum origin, reflecting the minimal energy associated with an electrical current and appears, as we will see, to be dominated by the effects of Coulomb interactions.

The geometric capacitance $C_H(\nu)$ depends on the width W of the sample, and of the structure and geometry of the quantum Hall edge channels (see Sec. IV of Suppplemental Material at [**?**]), through a length $\xi_H(\nu)$ proportional to the width $W_H(\nu)$ of a single channel. Following Ref. [27], $W_H(\nu) = (1 + \pi^2\alpha_{\rm eff}(\nu))\lambda_H(\nu)$, which is of the order of a few tens of nm for AlGaAs/GaAs quantum Hall systems. Finally, the inter-edge Coulomb interactions contribution to $v_{\rm eff}(\nu)$

$$\frac{v_{\rm d}(\nu)C_q(\nu)}{2C_H(\nu)} \simeq \frac{\sigma_H(\nu)}{2\pi\varepsilon_0\varepsilon_r}\ln\left(\frac{W}{\nu\xi_H(\nu)}\right) \tag{4}$$

is found to be linear in ν, because of its proportionality to the quantum Hall conductivity $\sigma_H(\nu)$, but with a logarithmic multiplicative correction which is a signature of Coulomb interactions.

We will now discuss how this expression and the experimental data enable us to rule out some models for $v_{\rm d}(\nu)$. We have considered two different models for the confining potential at the edge of the sample which leads to a different prediction for $v_{\rm d}(\nu)$: in Ref. [54], $v_{\rm d}(\nu) = \omega_c/k_F$ where $\omega_c = eB/m^*$ is the cyclotron frequency and $k_F = \sqrt{2\pi/n_S}$ the Fermi wave-vector. This leads to a dependence $v_{\rm d}(\nu) = v_{\rm d}/\nu$ whereas in Ref. [55], the gradient of the potential is proportional to $\hbar\omega_c/l_B$ where $l_B = \sqrt{\hbar/eB}$ is the magnetic length thereby leading to a scaling $v_{\rm d}(\nu) = v_{\rm d}/\sqrt{\nu}$.

Fig. 3 contains the first main quantitative result of this work, *i.e.* the quantum inductance as function of $1/\nu$ for configurations $B < 0$ ($B > 0$ configurations are analyzed in the Sec. V of Suppplemental Material at [**?**]). Values have been obtained from the reactance data depicted on Fig. 2 using the slope at low frequency of $f \mapsto X(f)$ datasets. Three configurations in which $L_{\rm pot}$ and $H_{\rm pot}$ are plugged to different contacts (see Fig. 3) and thus correspond to different l have been studied. The

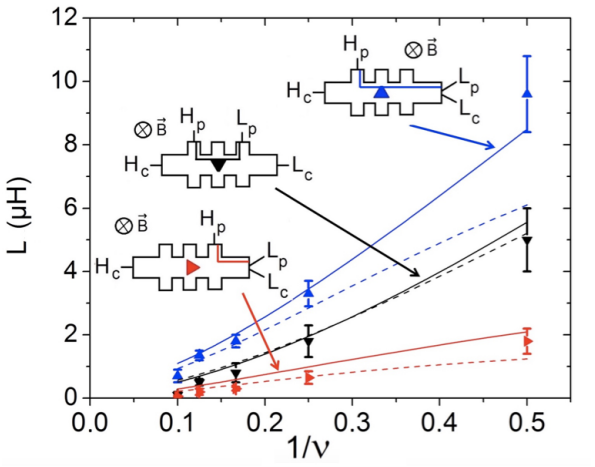

FIG. 3. (Color online) For measurement configurations with $B < 0$ corresponding to $l = 600\,\mu$m, $1000\,\mu$m and $1600\,\mu$m, the inductance increases with $1/\nu$. Dashed lines correspond to model $v_{\rm d}(\nu) = v_{\rm d}/\nu$ with $v_{\rm d} = 15$, 5 and 40 (in units of $10^5\,{\rm ms}^{-1}$) from top to bottom. The $v_{\rm d}(\nu) = v_{\rm d}/\sqrt{\nu}$ model leads to (solid lines) $v_{\rm d} = 6$, 3 and 17 in units of $10^5\,{\rm ms}^{-1}$ from top to bottom. The blue points corresponds to the experimental data displayed on Fig. 2.

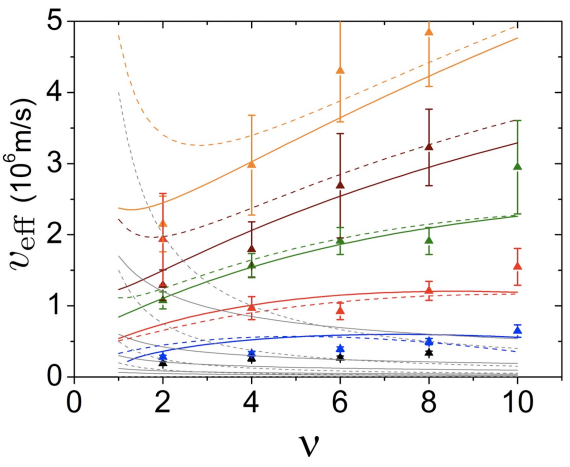

FIG. 4. (Color online) $v_{\rm eff}$ as a function of ν. Dashed curves correspond to $v_{\rm d}(\nu) = v_{\rm d}/\nu$ and full lines to $v_{\rm d}(\nu) = v_{\rm d}/\sqrt{\nu}$. Colored lines correspond to the expressions (1) taking into account inter-edge Coulomb interactions. Thin grey curves correspond to plots of the bare velocity $v_{\rm d}(\nu)$. The full lines have been obtained with (starting from the top curve): $v_{\rm d} = 17$, $v_{\rm d} = 6$ (fit of the data from Fig. 2), $v_{\rm d} = 3$, $v_{\rm d} = 1.2$ and $v_{\rm d} = 0.66$ in units of $10^5\,{\rm ms}^{-1}$. For the dashed lines, we have starting from the top curve: $v_{\rm d} = 40$, $v_{\rm d} = 15$, $v_{\rm d} = 5$, $v_{\rm d} = 2$ and $v_{\rm d} = 1$ in units of $10^5\,{\rm ms}^{-1}$.

main result is the dependence of the inductance on $1/\nu$ which involves a linear part (see Eq. (3a)) due to the presence of ν channels in parallel, but with a non-linear correction stemming from the ν-dependence of $v_{\rm d}(\nu)$ (see Eqs. (3b)) together with Coulomb interaction effects (see Eq. (4)). The different dependences of $v_{\rm d}(\nu)$ lead to different theoretical predictions. We find that the scaling $v_{\rm d}(\nu) = v_{\rm d}/\sqrt{\nu}$ is the best for describing the experimental data.

We have then extracted the velocity $v_{\rm eff}(\nu)$ using Eq. (3a) from each value of the inductance (see Fig. 4). This is the second main quantitative experimental result of this work. Each family of points corresponds to a specific sample configuration for which the sample has been heated up, re-bonded and cooled down again. These manipulations affect the electrostatic arrangement of charges at the edge, thereby modifying $v_{\rm d}$ from one experiment to the other. Fig. 4 presents predictions for $v_{\rm eff}(\nu)$ from Eq. (1) for different models for $v_{\rm d}(\nu)$. Similarly to the discussion of Fig. 3, the $\nu^{-1/2}$ scaling for $v_{\rm d}(\nu)$ gives the best reproduction of the experimental data. But a striking point is that in order to reproduce the experimental data, it is necessary to take into account the inter-channel Coulomb interactions: ignoring the interactions would correspond to using $v_{\rm d}(\nu)$ instead of $v_{\rm eff}$ in Eq. (3a). This is shown by the thin filled and dashed grey curves on Fig. 4, which clearly do not follow the experimental data. We thus interpret the ν-dependence of $v_{\rm eff}(\nu)$ when increasing ν from 2 to 10 (mostly linear with log-correction) as a strong indication of the dominant role of Coulomb interactions in these ungated samples.

Let us comment on the spread of values for $v_{\rm d}$ given in Fig. 4, which reflects the variability of the electrostatic environment in the samples from one experimental cooldown to another. A variation by a factor 25 is observed across all experiments (three higher curves for $B > 0$, all others for $B < 0$) but by only a factor 6 when considering only one orientation of B. This is still much larger than the relative change of the 2DEG density but $v_{\rm d}$ reflects the edge potential, which may vary more from one experiment to the other. As we use a shallow etching technique, the samples edges are very sensitive to any change of the electric potential landscape[56]. The values that we have obtained for $v_{\rm d}(\nu = 2)$ are compatible with estimates in the literature [57] for shallow etched samples. Moreover, our measurements of $v_{\rm eff}(\nu)$ are in the same range and qualitatively show a similar ν-dependence as the ones obtained in Ref. [58] for ungated samples by a time-of-flight technique.

To summarize, we have shown that, at low frequencies, a macroscopic quantum Hall bar is a perfect 1D conductor exhibiting a vanishing longitudinal resistance and a finite inductance. By fitting its dependence on ν and on the sample geometry using a simple long range effective Coulomb interaction model in the spirit of Büttiker *et al* [53], we have shown that it reflects the effective quantum inertia of charge carriers within the edges of the quantum Hall bar. Contrary to the case of superconductors where carrier inertia arises from the effective mass of the Cooper pairs, here it reflects how Coulomb interactions alter the propagation of low-frequency massless edge-magnetoplasmon modes. Remarkably, the experimental data can be understood using a simple model which is formally similar to the one used for gated nano-

fabricated samples [59**?**]: starting from chiral charge transport with bare velocity $v_{\rm d}(\nu)$, we include Coulomb interactions with the other edges via classical electrostatics and edge structure geometry from Ref. [27]. Going beyond this phenomenological but practical model would involve a multiscale treatment combining our approach to inter-channel interactions with a self-consistent microscopic approach solving the problem of electrons in the presence of intra-channel Coulomb interactions [60**?** , 61].

Finally, macroscopic samples may provide a rescaled test-bed for studying the scattering properties of edge-magnetoplasmons in 1 to 100 µm-sized samples. Studying a.c. transport properties of macroscopic samples up to radio-frequencies could thus open the way to realizing controlled quantum linear components for quantum nano-electronics in 1D edge channels, with possible applications to electron [62] and micro-wave quantum optics in ballistic quantum conductors [63].

ACKNOWLEDGMENTS

We warmly thank G. Fève and B. Plaçais (ENS Paris) and Ch. flindt (Aalto University) for useful discussions and suggestions, K. Ikushima (Tokyo University) for discussions at early stages of this work as well as the referees for important comments and clarifications on this manuscript. This work has been partly supported by ANR grant "1shot reloaded" (ANR-14-CE32-0017) and the French Renatech network.

[1] K. v. Klitzing, G. Dorda, and M. Pepper, Phys. Rev. Lett. **45**, 494 (1980).
[2] B. Halperin, Phys. Rev. B **25**, 2185 (1982).
[3] R. J. Haug, Semiconductor Science and Technology **8**, 131 (1993).
[4] M. E. Suddards, A. Baumgartner, M. Henini, and C. J. Mellor, New Journal of Physics **14**, 083015 (2012).
[5] C. I. des Poids et Mesures, "Représentation de l'ohm à partir de l'effet hall quantique," Recom. 2 (CI-1988) 77th Session (1988).
[6] B. Jeckelmann and B. Jeanneret, Reports on Progress in Physics **64**, 1603 (2001).
[7] F. J. Ahlers, B. Jeanneret, F. Overney, J. Schurr, and B. M. Wood, Metrologia **46**, R1 (2009).
[8] F. Delahaye, Metrologia **31**, 367 (1995).
[9] S. W. Chua, A. Hartland, and B. Kibble, IEEE Transactions on Instrumentation and Measurement **48**, 309 (1999).
[10] J. Schurr, B. Wood, and F. Overney, IEEE Transactions on Instrumentation and Measurement **54**, 512 (2005).
[11] M. E. Cage and A. Jeffrey, J. Res. Natl. Inst. Stand. Technol. **101**, 733 (1996).
[12] B. Jeanneret, B. D. Hall, H.-J. Bühlmann, R. Houdré, M. Ilegems, B. Jeckelmann, and U. Feller, Phys. Rev. B **51**, 9752 (1995).
[13] J. Schurr, J. Kučera, K. Pierz, and B. P. Kibble, Metrologia **48**, 47 (2011).
[14] P. J. Burke, IEEE Transactions on Nanotechnology **1**, 129 (2002).
[15] J. Kang, Y. Matsumoto, X. Li, J. Jiang, X. Xie, K. Kawamoto, M. Kenmoku, J. H. Chu, W. Liu, J. Mao, K. Ueno, and K. Banerjee, Nature Electronics **1**, 46 (2018).
[16] A. A. Annunziata, D. F. Santavicca, F. Frunzio, G. Catelani, M. J. Rooks, A. Frydman, and D. E. Prober, Nanotechnology **21**, 445202 (2010).
[17] J. Luomahaara, V. Vesterinen, L. Grönberg, and J. Hassel, Nature Communications **5**, 4872 (2014).
[18] G. Coiffard, K. F. Schuster, E. F. C. Driessen, S. Pignard, M. Calvo, A. Catalano, J. Goupy, and A. Monfardini, Journal of Low Temperature Physics **184**, 654 (2016).
[19] M. Büttiker, A. Prêtre, and H. Thomas, Phys. Rev. Lett. **70**, 4114 (1993).
[20] M. Büttiker, J. Phys.: Condens. Matter **5**, 9361 (1993).
[21] A. Prêtre, H. Thomas, and M. Büttiker, Phys. Rev. B **54**, 8130 (1996).
[22] J. Gabelli, G. Fève, J. Berroir, B. Plaçais, A. Cavanna, B. Etienne, Y. Jin, and D. Glattli, Science **313**, 499 (2006).
[23] J. Gabelli, G. Fève, T. Kontos, J.-M. Berroir, B. Plaçais, D. Glattli, B. Etienne, Y. Jin, and M. Büttiker, Phys. Rev. Lett. **98**, 166806 (2007).
[24] L. Song, J. Yin, and S. Chen, New Journal of Physics **20**, 053059 (2018).
[25] M. Büttiker, Phys. Rev **B 38**, 9375 (1988).
[26] S. M. Girvin and K. Yang, *Modern Condensed Matter Physics* (Cambridge university Press, 2019).
[27] D. Chklovskii, B. Shklovskii, and L. Glazman, Phys. Rev. B **46**, 4026 (1992).
[28] I. Aleiner and L. Glazman, Phys. Rev. Lett. **72**, 2935 (1994).
[29] J. Han and D. Thouless, Phys. Rev. B **55**, R1926 (1997).
[30] M. Hashisaka, H. Kamata, N. Kumada, K. Washio, R. Murata, K. Muraki, and T. Fujisawa, Phys. Rev. B **88**, 235409 (2013).
[31] N. Hiyama, M. Hashisaka, and T. Fujisawa, Applied Physics Letters **107**, 143101 (2015).
[32] B. Kibble and G. Rayner, *Coaxial AC bridges* (Taylor & Francis, 1984).
[33] *Agilent impedance measurement handbook* (Agilent Technologies Inc., 2009).
[34] M. Grayson and F. Fischer, Journal of Applied Physics **98**, 013709 (2005), https://doi.org/10.1063/1.1948529.
[35] C. Hernandez, C. Consejo, P. Degiovanni, and C. Chaubet, Journal of Applied Physics **115**, 123710 (2014).
[36] W. Desrat, D. K. Maude, L. B. Rigal, M. Potemski, J. C. Portal, L. Eaves, M. Henini, Z. R. Wasilewski, A. Toropov, G. Hill, and M. A. Pate, Phys. Rev. B **62**, 12990 (2000).
[37] J. Melcher, J. Schurr, F. m. c. Delahaye, and A. Hartland, Phys. Rev. B **64**, 127301 (2001).
[38] Here $R_{xx}(\omega)$ denotes the frequency dependant longitudinal dependence of the quantum Hall bar.

[39] I. Safi and H. Schulz, Phys. Rev. B **52**, R1740 (1995).
[40] I. Safi, Eur. Phys. J. **D 12**, 451 (1999).
[41] E. Bocquillon, V. Freulon, J. Berroir, P. Degiovanni, B. Plaçais, A. Cavanna, Y. Jin, and G. Fève, Nature Communications **4**, 1839 (2013).
[42] A. O. Slobodeniuk, I. P. Levkivskyi, and E. V. Sukhorukov, Phys. Rev. B **88**, 165307 (2013).
[43] D. C. Glattli, E. Y. Andrei, G. Deville, J. Poitrenaud, and F. I. B. Williams, Phys. Rev. Lett. **54**, 1710 (1985).
[44] G. Sukhodub, F. Hohls, and R. J. Haug, Phys. Rev. Lett. **93**, 196801 (2004).
[45] I. Safi and H. Schulz, in *Quantum Transport in Semiconductor Submicron Structures*, edited by B. Kramer (Kluwer Academic Press, Dordrecht, 1995) p. 159.
[46] H. Steinberg, G. Barak, A. Yacobi, L. Pfeiffer, K. West, B. Halperin, and K. Le Hur, Nature Physics **4**, 116 (2008).
[47] H. Kamata, N. Kumada, M. Hashisaka, K. Muraki, and T. Fujisawa, Nature Nanotechnology **9**, 177 (2014).
[48] P. Brasseur, N. H. Tu, Y. Sekine, K. Muraki, M. Hashisaka, T. Fujisawa, and N. Kumada, Phys. Rev. B **96**, 081101 (2017).
[49] P. Degiovanni, C. Grenier, G. Fève, C. Altimiras, H. le Sueur, and F. Pierre, Phys. Rev. B **81**, 121302(R) (2010).
[50] C. Cabart, B. Roussel, G. Fève, and P. Degiovanni, Phys. Rev. B **98**, 155302 (2018).
[51] R. Rodriguez, F. Parmentier, D. Ferraro, P. Roulleau, U. Gensser, A. Cavanna, M. Sassetti, F. Portier, D. Mailly, and P. Roche, Nature Communications **11**, 2426 (2020).
[52] A. Delgard, B. Chenaud, D. Mailly, U. Gennser, K. Ikushima, and C. Chaubet, Physica Status Solidi B **256**, 1800548 (2019), https://onlinelibrary.wiley.com/doi/pdf/10.1002/pssb.201800548.
[53] T. Christen and M. Büttiker, Phys. Rev. B **53**, 2064 (1996).
[54] S. A. Mikhailov, "Edge and inter-edge magnetoplasmons in two-dimensional electron systems," in *Edge Excitations of Low-Dimensional Charged Systems*, Horizons in World Physics, Vol. 236, edited by O. Kirichek (Nova Science Publishers, Inc., NY, 2000) Chap. 7, pp. 171 – 198.
[55] C. Chaubet and F. Geniet, Phys. Rev. B **58**, 13015 (1998).
[56] Additional results obtained on samples from different wafers are presented in Sec. V of Suppplemental Material at [**?**] provide additional evidence of the robustness of our analysis.
[57] P. Roulleau, F. Portier, D. Glattli, P. Roche, A. Cavanna, G. Faini, U. Gennser, and D. Mailly, Phys. Rev. Lett. **100**, 126802 (2008).
[58] N. Kumada, H. Kamata, and T. Fujisawa, Phys. Rev. B **84**, 045314 (2011).
[59] M. Hashisaka, K. Washio, H. Kamata, K. Muraki, and T. Fujisawa, Phys. Rev. B **85**, 155424 (2012).
[60] P. Armagnat, A. Lacerda-Santos, B. Rossignol, C. Groth, and X. Waintal, SciPost Phys. **7**, 31 (2019).
[61] G. Roussely, E. Arrighi, G. Georgiou, S. Takada, M. Schalk, M. Urdampilleta, A. Ludwig, A. D. Wieck, P. Armagnat, T. Kloss, X. Waintal, T. Meunier, and C. Bäuerle, Nature Communications **9**, 2811 (2018).
[62] E. Bocquillon, V. Freulon, F. Parmentier, J. Berroir, B. Plaçais, C. Wahl, J. Rech, T. Jonckheere, T. Martin, C. Grenier, D. Ferraro, P. Degiovanni, and G. Fève, Ann. Phys. (Berlin) **526**, 1 (2014).
[63] A. L. Grimsmo, F. Qassemi, , B. Reulet, and A. Blais, Phys. Rev. Lett. **116**, 043602 (2016).